Human PIEZO1: Removing Inactivation

Chilman Bae, Philip A. Gottlieb, and Frederick Sachs*
Department of Physiology and Biophysics and The Center for Single Molecule Biophysics, State University of New York at Buffalo, Buffalo, New York

ABSTRACT PIEZO1 is an inactivating eukaryotic cation-selective mechanosensitive ion channel. Two sites have been located in the channel that when individually mutated lead to xerocytotic anemia by slowing inactivation. By introducing mutations at two sites, one associated with xerocytosis and the other artificial, we were able to remove inactivation. The double mutant (DhPIEZO1) has a substitution of arginine for methionine (M2225R) and lysine for arginine (R2456K). The loss of inactivation was accompanied by ~30-mmHg shift of the activation curve to lower pressures and slower rates of deactivation. The slope sensitivity of gating was the same for wild-type and mutants, indicating that the dimensional changes between the closed and open state are unaffected by the mutations. The unitary channel conductance was unchanged by mutations, so these sites are not associated with pore. DhPIEZO1 was reversibly inhibited by the peptide GsMTx4 that acted as a gating modifier. The channel kinetics were solved using complex stimulus waveforms and the data fit to a three-state loop in detailed balance. The reaction had two pressure-dependent rates, *closed* to *open* and *inactivated* to *closed*. Pressure sensitivity of the opening rate with no sensitivity of the closing rate means that the energy barrier between them is located near the open state. Mutant cycle analysis of inactivation showed that the two sites interacted strongly, even though they are postulated to be on opposite sides of the membrane.

INTRODUCTION

PIEZO1 is a eukaryotic mechanosensitive cation-selective channel (1–3) of ~2500 amino acids containing 30 putative transmembrane domains (1,4,5). It has electrophysiological properties similar to many endogenous cationic mechanosensitive ion channels (MSCs), with a reversal potential around 0 mV, voltage-dependent inactivation, and inhibition by the peptide GsMTx4 (6,7). PIEZO1 forms homotetrameric aggregates (2), but it is not known whether the pore is located in the monomers or at the interfaces.

The channel is sensitive to its physical environment because the gating kinetics are not identical in patch and whole-cell recordings (8). The channels appear to exist in physical domains that can be fractured at stresses below the lytic strength of the bilayer (7). The domains might consist of clusters of channels, lipid phases, or cytoskeletal corrals (9).

Mutations (M2225R and R2456H) that produce human hereditary xerocytosis (an autosomal dominant anemia) have slower inactivation rates than wild-type (WT) (7,10,11) and an increased latency to activation (7). The longer open times due to slow inactivation will produce the larger cation fluxes that seem to be associated with hereditary xerocytosis (7,10,11), but longer latencies will reduce the flux for transient stimulations such as passage through capillaries. The mutations do not seem to act via changes in residue charge because the conservative mutation of arginine to lysine at position 2456 slowed inactivation.

A double mutant, DhPIEZO1, substitutes an arginine for a methionine at position 2225 (M2225R), which is associated with hereditary xerocytosis, and a lysine for an arginine at position 2456 (R2456K), which we created. The single-site mutants inactivated slower than WT (7), but the double mutant did not inactivate at all. To examine whether the two sites interacted to produce the loss of inactivation, we did a mutant cycle analysis and estimated the free energy for inactivation for WT, single-site mutants, and the double mutant. The analysis shows a strong interaction.

Other properties of DhPIEZO1 were similar to WT, including the near-zero Na/K reversal potential and inhibition by GsMTx4. The gating curves (the Boltzmann relationship of open probability vs. pressure) showed that the dimensional change between closed and open states was similar to WT, although the midpoint of the gating curve was shifted to lower pressures. The channel kinetics of all channel types, even for complex stimuli, could be fit with a simple three-state closed loop model (closed–open–inactivated) in detailed balance with only two pressure-dependent rates.

MATERIALS AND METHODS

The bath solution contained (in mM) 150 NaCl, 5 KCl, 1 $MgCl_2$, 2.5 $CaCl_2$, 10 HEPES, pH 7.4 (adjusted with NaOH). The pipette solution contained (in mM) 150 CsCl, 10 HEPES, 5.0 EGTA, 1.0 $MgCl_2$, 1.0 $CaCl_2$, pH 7.3 (adjusted with CsOH), or 150 KCl, 10 HEPES, 0.25 EGTA, 0.5 $MgCl_2$, pH 7.3 (adjusted with KOH). Patch pipettes had resistances of 2–5 MΩ. The mechanical stimulus for patches was pipette suction for cell-attached patches and pipette pressure for outside-out patches. All pressure stimuli were applied by a high-speed pressure clamp (ALA Scientific Instruments, Farmingdale, NY). Whole-cell and patch-clamp currents were recorded using an Axopatch 200B amplifier (Axon Instruments), sampled at 10 kHz,

Submitted May 8, 2013, and accepted for publication July 16, 2013.

*Correspondence: Sachs@buffalo.edu

Editor: Michael Pusch

0006-3495/13/08/0880/7 $2.00

http://dx.doi.org/10.1016/j.bpj.2013.07.019

and low pass filtered at 1 kHz. Patch capacitance and conductance were measured as previously described (12,13) using an EG&G 5208 two-phase lock-in analyzer (Oak Ridge, TN).

The dose–response data were fit to a Boltzmann relationship, and when we had two different types of channels in a patch, the data were fit to the sum of two Boltzmann functions:

$$I = A + Im_1 \times \left[1 - \frac{1}{1 + e^{(q_1 \times (p_1 - p))}}\right] + Im_2 \times \left[1 - \frac{1}{1 + e^{(q_2 \times (p_2 - p))}}\right],$$

where Im_i is the maximum available current for channel type i, p_i is the pressure at half activation, q_i is the slope sensitivity, and A is an instrumental offset.

Whole-cell mechanical stimulation used a fire-polished glass pipette (diameter of 2–4 μm) positioned at an angle of 30° with respect to the cover glass to press on voltage clamped cells. The probe was coarsely positioned ~15 μm above the cell; from that position, we applied a trapezoidal downward waveform with a piezoelectric stage (P-280.20 XYZ NanoPositioner, Physik Instrumente). The indentation depth with 40-nm resolution was controlled using LabVIEW. The probe velocity was 0.15 μm/ms during transitions, and the indentation was held constant for 300 ms. Currents were generally recorded at a holding potential of −60 mV at room temperature. Hypotonic swelling was initiated by adding distilled water in equal volume to the bath solution.

To compute the channel kinetics, we applied a series of square suction pulses with variable off times (3.0, 2.0, 1.0, 0.5, 0.25, 0.1 s, and the reverse) usually in the cell-attached mode. These multichannel currents were analyzed using the MAC routine of QuB software (www.qub.buffalo.edu).

HEK-293 cells were transfected with 750 ng cDNA using Fugene (Roche Diagnostic, Indianapolis, IN) according to manufacturer's specification and transfected cells were tested 24–48 h later. The peptide GsMTx4 was synthesized, folded, and purified as previously described (14) and applied through an ALA perfusion system. Data acquisition and stimulation were all controlled by QUBIO software (www.qub.buffalo.edu).

RESULTS

Whole-cell data

At a given membrane potential, the currents increased with indentation depth (Fig. 1, *A* and *B*). In contrast to the WT channel (Fig. 1 *A*) and the single-site mutants (M2225R and R2456K) (7) that displayed faster or slower inactivation, respectively, DhPIEZO1 produced a steady-state current with sustained indentation (Fig. 1 *B*). DhPIEZO1 currents are mechanically sensitive, have no inactivation, and relative to WT, the channels are sensitized toward the open state. The fact that the DhPIEZO1 current persisted in steady state suggests that in the domains containing the channels there is no time-dependent adaptation of the local stimulus (13,15).

Osmotic pressure is often applied as an alternative stimulus to direct mechanical stimulation, but much of the osmotic stress is contained in the deep cytoskeleton, not the bilayer (16), so osmotic pressure is not an equivalent stimulus to direct stress. Nonetheless, we have found that hypoosmotic

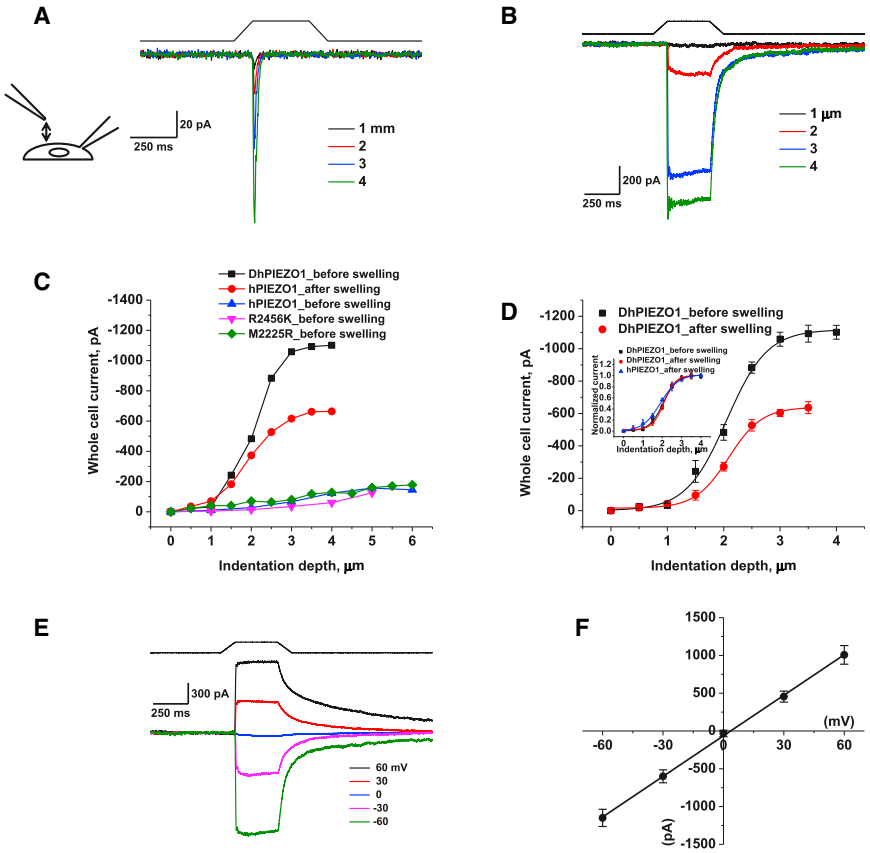

FIGURE 1 DhPIEZO1 does not inactivate. *(A)* Whole-cell currents of WT hPIEZO1 rapidly inactivate. *(B)* Whole-cell currents of DhPIEZO1 as a function of indentation depth showed no inactivation. Note the slow rate of deactivation after the stimulus is removed. *(C)* WT channels are sensitive to hypotonic swelling. Prior to swelling, there was less current for the same incremental indentation than after swelling. Also shown is the response of DhPIEZO1 prior to swelling. *(D)* Comparison of DhPIEZO1 responses before and after hypotonic swelling with 50% osmolarity. The inset shows the same data normalized. The sensitivity to indentation is similar, suggesting that the channels are already near a saturated level of stress in the resting state. *(E)* Deactivation is extremely slow and voltage independent. Deactivation for this channel may represent the kinetics of domain reformation rather than channel kinetics. *(F)* The I/V curve of peak currents shows a reversal potential near 0 mV for DhPIEZO1, indicating that the mutations do not affect the pore.

pressure increased the sensitivity of WT hPIEZO (Fig. 1 *C*) similar to results reported for the mouse channel (mPIEZO1) (8). In contrast, DhPIEZO1 proved insensitive to cell swelling, even when 50% distilled water was added to the bath (Fig. 1, *C* and *D*). This implies that the resting stress in the channel (prestress) is nearly saturated.

Because the rate of inactivation in WT and single-site mutants is voltage sensitive (1,6–8), we examined DhPIEZO1 from −60 to +60 mV. Fig. 1 *E* shows that the rate of inactivation was close to zero at all potentials. DhPIEZO1 *deactivation* was extremely slow relative to that of single-site mutants and WT, suggesting a structural correlation between inactivation and deactivation. All channel types had a similar ionic selectivity with a Na/K reversal potential of ~0 mV (Fig. 1 *F*), so that the mutations are not likely to be located near the pore.

Patch data

Cell-attached patches of DhPIEZO1 are mechanically sensitive and showed no inactivation, but had an increased latency for activation. The steady-state gating curve of DhPIEZO1 (Fig. 2 *A*) in patches was well fit by a Boltzmann function of $I = A + I_{max} \times (1 - 1/(1 + \exp(q \times (p - p_{1/2}))))$, where I_{max} is the maximum available current, p is the pressure, $p_{1/2}$ is the pressure at half activation, and q is the slope sensitivity to pressure. For DhPIEZO1, $p_{1/2} = -9.9 \pm 0.6$ mmHg, and the slope sensitivity, q, was 0.15 ± 0.01 mmHg^{-1} (*SD*, $n = 12$). For WT, the midpoint $p_{1/2} = -38.1 \pm 0.4$ mmHg and $q = 0.15 \pm 0.01$ mmHg^{-1} (*SD*, $n = 18$) comparable to previously measured values (7). The q-values of all channel types were the same, implying that the dimensional changes between the closed and open states are the same. The decrease in $p_{1/2}$ with constant q implies that the mutations added resting stress to the structure (prestress), favoring the open state. In terms of energy, the data indicate that the mutations decreased the energy of the open state while maintaining the difference in energy between the closed state and the barrier peak.

To calibrate the absolute sensitivity of DhPIEZO1, we cotransfected cells with a eukaryotic-expressing bacterial MSC called MscL that has been calibrated in bilayers (17,18). These cotransfection data were fit to the sum of two Boltzmanns, simultaneously solving for q and $p_{1/2}$ for both channels in the same patch (see *inset* in Fig. 2 *B*). The ratio of slope sensitivities for DhPIEZO1 to MscL was 0.98 ($n = 5$), so that both channels had similar dimensional changes between the closed and open states, equivalent to 20 nm^2 of in-plane area (17,19).

DhPIEZO1 was highly sensitive to the absolute level of pressure as a result of the leftward shift of the dose–response curve for pressure. A typical single-channel recording (Fig. 3 *A*) shows that a 3-mmHg change of suction, from −12 to −15 mmHg, resulted in a significant change in the number of active channels. These data were fit to a

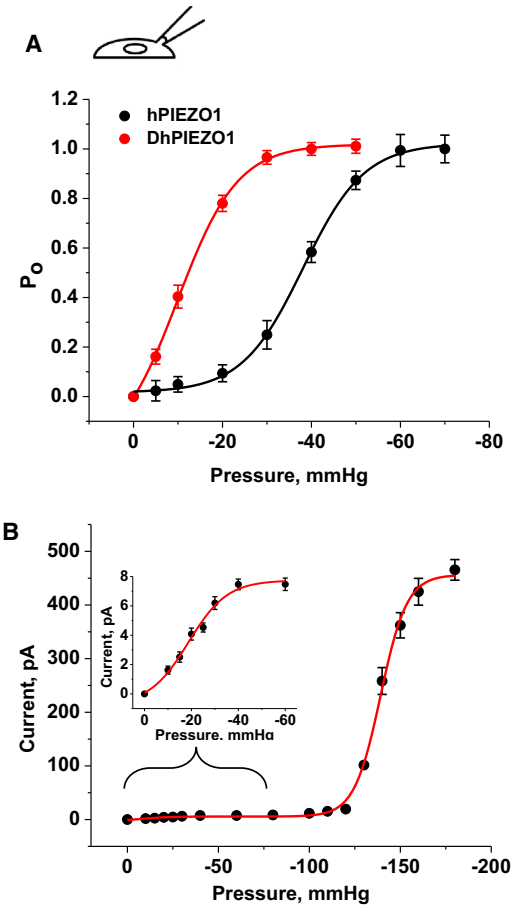

FIGURE 2 *(A)* The gating curve as a function of pressure fit to a Boltzmann. $p_{1/2}$ and the slope sensitivity q are indicated in the table. q is a measure of the dimensional change between closed and open states. q is the same for DhPIEZO1 ($n = 12$), WT ($n = 18$), and the single-site mutants, implying that the mutations have no effect on the key activation processes. However, $p_{1/2}$ was left-shifted relative to WT, representing a change in the intrinsic stress of the channel environment favoring the opening state. *(B)* To calibrate the absolute stress sensitivity, we cotransfected cells with bacterial MscL (7) and DhPIEZO1. Fit to a sum of two Boltzmanns, the slope sensitivities of both channels were nearly identical ($n = 5$), meaning that the dimensional changes of both channels are similar and also similar to WT and single-site mutants. The dimensional changes are equivalent to an in-plane area change of 20 nm^2.The inset shows an expansion of the region containing DhPIEZO1's response.

two-state model with a pressure-dependent opening rate and the same slope sensitivity as WT (Fig. 3 *A*). This extreme sensitivity is interesting considering that the resting patch is already under a large resting tension on the order of 1 to 2 mN/m because of adhesion of the gigaseal (15,20,21). Consistent with the higher absolute sensitivity of DhPIEZO1, we observed an increase in spontaneous openings (Fig. 3 *B*).

In contrast to WT channels that had no measurable latency for activation, DhPIEZO1 had a pronounced latency of ~250–350 ms followed by sudden activation (Fig. 3, *B* and *C*). The kinetics of the activation cannot be fit by simply adding more closed states prior to opening. We have proposed that the observed latency represents the time required

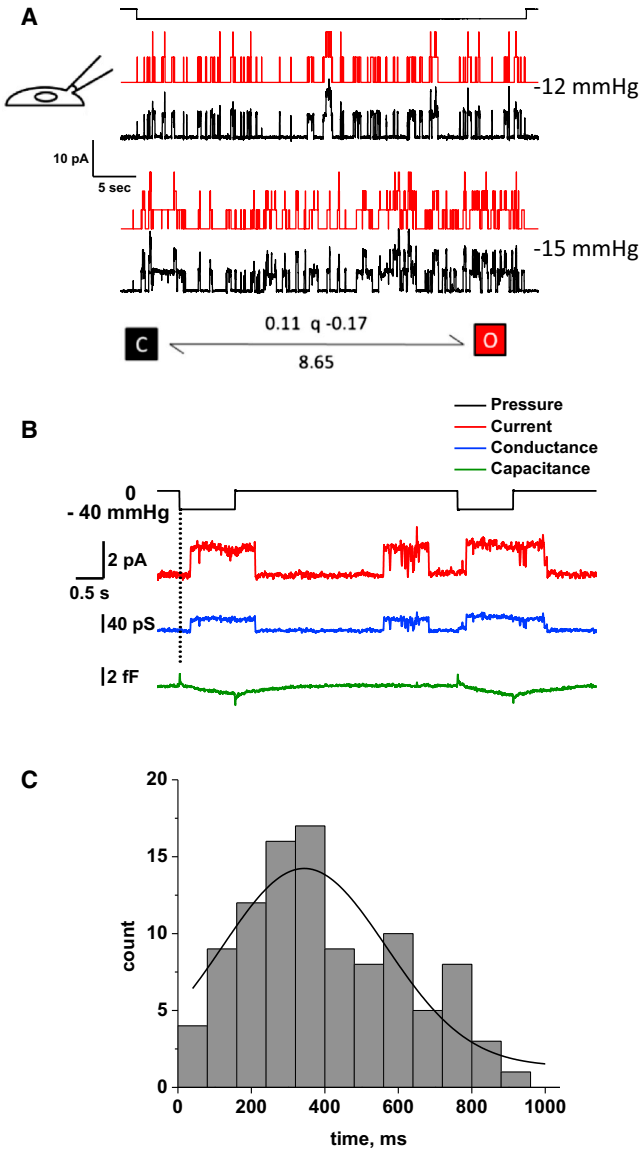

FIGURE 3 *(A)* DhPIEZO1 single-channel currents show high pressure sensitivity because of the left shift in the gating curve. The current trace is shown in black and the theoretical fit is in red. With a change of only 3 mmHg, there is a significant increase in the number of open channels. The kinetics are well fit by a two-state model with only the activation rate being pressure dependent. *(B)* Single-channel currents of DhPIEZO1 have a pronounced latency for activation, and this occurs with no significant change in patch capacitance, suggesting that the latency does not arise from large changes in the patch structure. The capacitance measuring noise level was 0.12 fF RMS, equivalent to ~0.012 μm^2 (assuming a specific capacitance of 1 $\mu F/cm^2$, or 10 $fF/\mu m^2$). Note the spontaneous (background) channel openings of DhPIEZO1 during the recording that is a result of its higher absolute sensitivity and tension from the gigaseal. *(C)* The distribution of latencies fit to a Gaussian gives a mean latency of 344 ± 133 ms. We attribute these latencies to the time required for domain fracture under stress.

for the domain boundary to fracture and to change the stress on the channels (7). A change in the domain, such as fracturing a caveolus, might produce a change in area and hence a change in patch impedance. We tried to measure such a change (12,13) but we observed none (Fig. 3 *B*). The measurement noise level placed an upper limit on any area change to $< 0.01\ \mu m^2$. This suggests that the domain fracture probably did not involve opening of a vesicular structure such as a caveolus.

Inhibition by GsMTx4

PIEZO1 currents are reversibly inhibited by the D-enantiomer of GsMTx4, a specific inhibitor of cationic MSCs (6,22). The lower graph of Fig. 4 *A* shows whole-cell peak

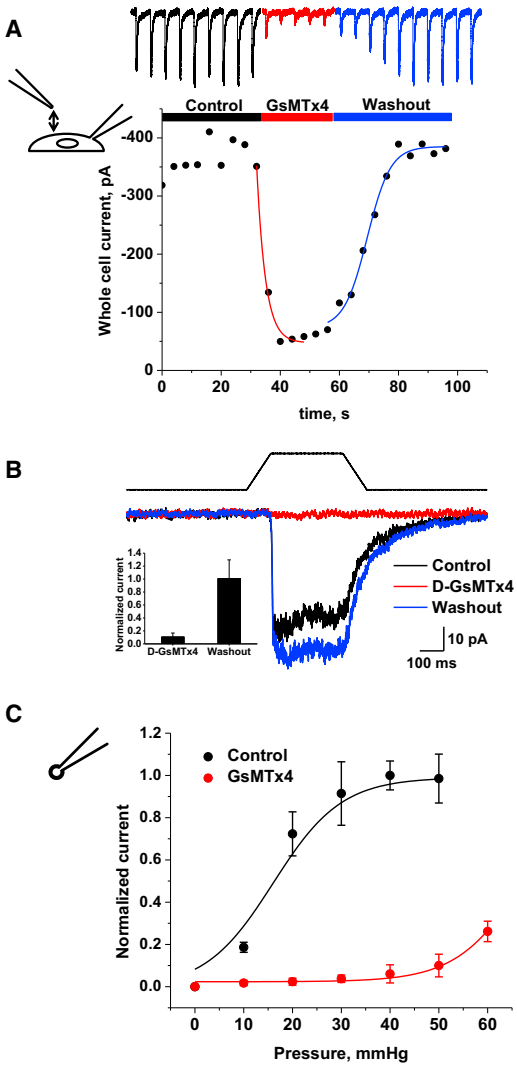

FIGURE 4 DhPIEZO1 channels in whole-cell patches were reversibly inhibited by 10 μM extracellular D-GsMTx4. *(A)* By fitting exponentials, we extracted a mean association time constant of 3.0 ± 0.6 s and a mean dissociation time constant of 13.4 ± 0.8 s ($n = 4$). The estimated association and dissociation rates are $2.6 \times 10^4\ M^{-1}\ s^{-1}$ and $0.08\ s^{-1}$, respectively, and the equilibrium constant calculated from the ratio is K_D ~3 μM. *(B)* D-GsMTx4 inhibition of DhPIEZO1 in the absence of inactivation. This suggests that the mechanism of action of D-GsMTx4 does not involve inactivation domains. The bar graph *(inset)* shows the average peak currents ± *SD* ($n = 3$) illustrated in Fig. 4 *B*. *(C)* The dose–response relationship shifts to higher stress with GsMTx4, as expected for a gating modifier (12).

currents as a function of time from GsMTx4 exposure through washout. From single exponential fits, the association time constant was 3.0 ± 0.63 s and the dissociation time constant was 13.4 ± 0.76 s. The ratio gives an equilibrium affinity of ~3 μm. Fig. 4 *B* shows that D-GsMTx4 inhibition occurs in the absence of inactivation so that the peptide does not seem to interact with the inactivation domain(s) of the channel. At −60 mV, 10 μM GsMTx4 caused an 89% reduction in peak current (Fig. 4 *B*). In outside-out patches (Fig. 4 *C*), the inhibition was >90%. GsMTx4 is a gating modifier acting on closed channels (6), and we estimated its efficacy to be equivalent to ~60 mmHg by the increase of suction required to obtain equal channel activity with and without GsMTx4.

Channel kinetics: Cell-attached patches

We stimulated the patch with a series of square suction pulses with varying time intervals between them (typically 3.0, 2.0, 1.0, 0.5, 0.25, 0.1 s, and the reverse). The response to the entire sequence could be fit using the MAC routine of QuB (www.qub.buffalo.edu). This nonstationary approach has many advantages over traditional single- or double-step analyses in that the responses need not reach equilibrium before the next pulse is applied. Furthermore, the fit is a global optimum for the entire sequence (i.e., the series is treated as a single stimulus; see Fig. 5 *A*).

DhPIEZO1 kinetics were fit with a simple three-state loop model (closed, open, and inactivated) in detailed balance (at all stimuli). To simplify comparison of the kinetics to WT and single-site mutations that required three states, we fit the DhPIEZO1 kinetics to the three-state model even though it had no inactivation. Detailed balance in a loop requires a minimum of two pressure-dependent rates, and we found we could satisfy that constraint with a pressure-dependent opening rate and inactivated-closed rate (Fig. 5 *B*). One of the most striking results of the kinetic analysis was that all channel types had identical slope sensitivities, q = 0.15 ± 0.005 $mmHg^{-1}$ (Fig. 5 *B*) so that the conformational change between the closed and open states of all channels was identical. Furthermore, all the channels had to be in domains with similar local stress. The preexponential coefficients of the activation rates were 10×10^{-3} s^{-1}, 4.62×10^{-3} s^{-1}, 6.13×10^{-3} s^{-1}, and 3.28×10^{-3} s^{-1} in hPIEZO1, M2225, R2456K, and DhPIEZO1, respectively, at −60mV. The mutations had little or no effect on the

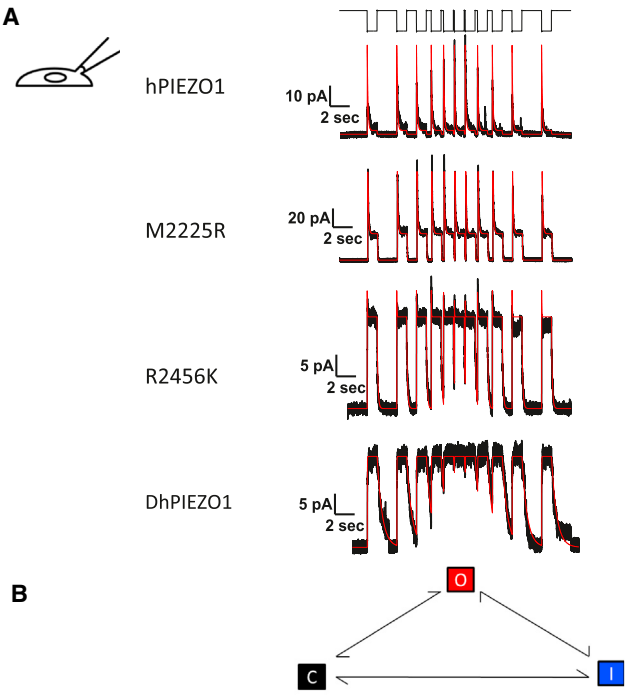

st1 → st2		hPIEZO1	M2225R	R2456K	DhPIEZO1
C	O	0.01 q -0.16	4.62e-3 q -0.15	6.13e-3 q -0.15	3.28e-3 q -0.15
O	C	1.12	1.45	8.86	2.06
O	I	8.59	12.19	2.84	5.40E-04
I	O	1.19	4.40	115.1	141.46
I	C	73.77 q 0.16	153.40 q 0.15	4408.20 q 0.15	1888.80 q 0.15
C	I	3.28	1.35	0.08	1.22E-05

FIGURE 5 Channel kinetics. *(A)* Multichannel currents for different types of channels. The stimulus was a series of square pressure pulses applied with varying off intervals (typically 3.0, 2.0, 1.0, 0.5, 0.25, 0.1 s, and the reverse, *top trace*). Pressure pulses were 0 to −70 mmHg for HPIEZO1, 2555R PIEZO1, and 2456K PIEZO. For DhPIEZO1, they were 0 to –40 mmHg. The data trace is in black and the QuB fit in red. Notice how hPIEZO1 effectively summed currents from the applied stresses at short off-times of the stimulus. However, the mutant M2225R tended to accumulate inactivation in the same part of the stimulus (lower peaks at shortest resting intervals), but this can be accounted for simply by a change in the rate constants and requires no additional states. The kinetic parameters that characterize the behavior of all channels are presented in *(B)*. *(B)* Tabulation of the quantified kinetics with the three-state loop in detailed balance. The states are named C =closed state, O = open state, and I = inactivated state. Although DhPIEZO1 does not appear to have an inactivated state, we included it for consistency to better compare the models. The pressure dependence for all channel types is contained in the opening rate and the inactivated-closed rate. The pressure sensitivity of the rates is indicated by the parameter q [$mmHg^{-1}$]. q was consistent across all types of channels at ~0.15 so that the conformation associated with opening in all channel types is identical. The DhPIEZO1 trace ends with a jump that is probably closure of the last open channel.

0-mmHg opening rates (the preexponential coefficients). Because the preexponential term contains the entropy of activation, we infer that the mutations also did not change that component of the free energy.

Inactivation is fast in hPIEZO1, M2225R, and R2456K (12.7 s^{-1}, 9.8 s^{-1}, 12.4 s^{-1} at −60 mV, respectively), and DhPIEZO1 effectively did not inactivate ($< 1.6 \times 10^{-6}$ s^{-1} at −60 mV). When we examined deactivation, hPIEZO1 and M2225R were faster than the pressure clamp's response time, but R2456K was slow enough to measure (6.2 s^{-1}), and DhPIEZO1 was even slower (2.4 s^{-1}). Deactivation represents the process of going from open to closed and is characterized by the energy difference between the open state and the energy barrier between the open and closed state. If the change in deactivation rate was due to a change in barrier height, we would expect that the slope sensitivity for opening, q, would also change, but it did not, so the change in deactivation rate appears to represent changes in the open state energy. Slow deactivation of DhPIEZO1 may represent reforming of the domain, the inverse of fracturing. The C-terminal domain, where the mutations are located, is presumably involved in domain creation (7).

To explore whether the two mutation sites were independent, we did a mutant cycle analysis of inactivation (23). If the two sites were independent, the free energy difference for inactivation of DhPIEZO1 should be the sum of the energies of the single mutants. However, the data showed that the energy of the dual mutant is much larger than the sum of the two single mutant energies, so they must be interacting. The basic calculation is as follows, where ΔG_i is the free energy with mutation of residue i, and $\Delta\Delta G_i$ is the free energy changes with mutation of residue i.

$$\begin{aligned}
\Delta\Delta G_{2225} &= \Delta G_{2225} - \Delta G_{\mathrm{WT}}.\\
\Delta\Delta G_{2456} &= \Delta G_{2456} - \Delta G_{\mathrm{WT}}.\\
\Delta\Delta G_{\mathrm{DhPIEZO1}} &= \Delta G_{\mathrm{DhPIEZO1}} - \Delta G_{\mathrm{WT}}.
\end{aligned}$$

$$\begin{aligned}
\Delta G &= \Delta\Delta G_{\mathrm{DhPIEZO1}} - (\Delta\Delta G_{2225} + \Delta\Delta G_{2456})\\
&= \Delta G_{\mathrm{DhPIEZO1}} + \Delta G_{\mathrm{WT}} - \Delta G_{2225} - \Delta G_{2456}\\
&= -k_B T \times \left[\ln\left(\frac{5.4 \times 10^{-4}}{141.46}\right) + \ln\left(\frac{8.59}{1.19}\right)\right.\\
&\quad \left. - \ln\left(\frac{12.19}{4.40}\right) - \ln\left(\frac{2.84}{115.10}\right)\right]\\
&= 7.82\ k_B T.
\end{aligned}$$

The difference of free energy $\Delta G = 7.82\ k_B T$ shows that the sites are not independent despite on apparently opposites sides of the bilayer (7).

DISCUSSION

A striking feature of activation is that the slope sensitivity q was identical for all channel types. This means that the energy between the closed and open states was identical. Perhaps even more surprising is that this also implies that the local stresses sensed by the channel were identical: The domains were similar enough that the internal stresses were the same. The free energy of gating is well approximated by $\Delta G = T\Delta A$, where T is the local tension and ΔA is the change of in-plane area so that a change in T will produce a change in ΔG. The data on DhPIEZO1 also show that activation is effectively uncoupled from inactivation.

The kinetics of all mutants could be fit with the three-state loop model with the same two pressure-dependent rates so that the mutations did not appear to introduce any new states (Fig. 5). The fact that the kinetics of all the channels could be fit with a pressure-sensitive opening rate and a pressure-independent closing (deactivation) rate means that the energy barrier between the states is located close to the open state.

Because the slope sensitivity for activation was constant across all mutations, slowing the inactivation rate increases the channel open time for a transient stimulus. We have previously shown that PIEZO1 inactivates and does not adapt (8). To slow inactivation, one elevates the energy barrier between the open and inactivated states. But because the slope sensitivity for activation, q, was unchanged among the mutants, the difference in energy between the closed state and the barrier peak has to remain constant. Thus, the slowing of inactivation appears to represent a lowering of the energy of the open state.

The fact that the mutations caused changes in both the inactivation rate and the deactivation rate suggests that the two processes are coupled. A channel with fast inactivation, such as the WT, also has fast deactivation. When inactivation is slow (DhPIEZO1), then deactivation is slow. We previously suggested that inactivation may reflect an increased interaction between monomers to form clusters (domains) and that the regions of the channel altered by the mutations are also involved in intermonomer binding (7). DhPIEZO1 channels with no inactivation and slow deactivation may exist in loose, easily fractured clusters. The DhPIEZO1 kinetic behavior is quite similar to what we observed with the removal of the C-terminal domain (7).

Mutant cycle analysis of inactivation using WT, single-site mutants, and DhPIEZO1 (23) showed that the two sites interacted with ~8 $k_B T$ of energy (Fig. 6). What is the mechanism of coupling? It could be part of a common flexible region of the channel or possibly affect binding to the cytoskeleton and extracellular matrix, but that is doubtful given that we have previously demonstrated that disruptors of the cytoskeleton, such as CytochalasinD, disrupt whole-cell currents. However, we know that the channels are still present because patches from those cells show functional channels. The cytoskeletal disruptors probably do not affect the channel itself but more likely the mechanical pathways that affect the local distribution of stress (8). A lack of interaction with cytoskeletal proteins is supported by

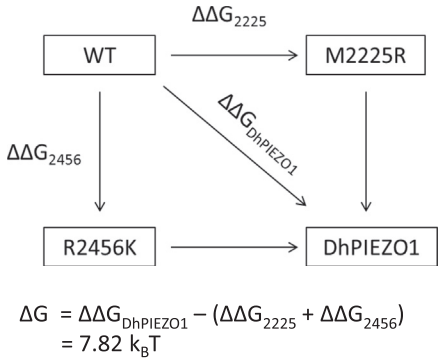

FIGURE 6 Mutant cycle analysis. The energy difference between open and inactivated states for WT, single-site mutants, and DhPIEZO1. The free energy change in DhPIEZO1 ($\Delta\Delta G_{\mathrm{DhPIEZO1}}$) is larger than the sum of free energy changes for the two single mutants by ~8 k_BT, showing that the sites are not independent but exhibit positive cooperativity.

mass-spectrum analysis of mPIEZO1 that shows no additional proteins bound to the purified channel (2).

DhPIEZO1 may be a good candidate for developing a high throughput screen for inhibitors of PIEZOs. Given that it lacks inactivation, a persistent mechanical stimulus to DhPIEZO1 will induce a persistent calcium influx, making the assay insensitive to variations in the rates of inactivation. Furthermore, inhibition by the specific reagent GsMTx4 is a positive control.

This work was supported by the National Institutes of Health, Department of Defense, and the Children's Guild of Buffalo. We are grateful to Joanne Pazik and Lynn Zeigler for expert technical assistance on the molecular biology and Julia Doerner from David Clapham's laboratory for sharing the eukaryotic vector for expression of the MscL.

REFERENCES

1. Coste, B., J. Mathur, …, A. Patapoutian. 2010. Piezo1 and Piezo2 are essential components of distinct mechanically activated cation channels. *Science.* 330:55–60.
2. Coste, B., B. Xiao, …, A. Patapoutian. 2012. Piezo proteins are pore-forming subunits of mechanically activated channels. *Nature.* 483:176–181.
3. Kim, S. E., B. Coste, …, A. Patapoutian. 2012. The role of Drosophila Piezo in mechanical nociception. *Nature.* 483:209–212.
4. Gottlieb, P. A., and F. Sachs. 2012. Piezo1: properties of a cation selective mechanical channel. *Channels (Austin).* 6:214–219.
5. Nilius, B., and E. Honoré. 2012. Sensing pressure with ion channels. *Trends Neurosci.* 35:477–486.
6. Bae, C., F. Sachs, and P. A. Gottlieb. 2011. The mechanosensitive ion channel Piezo1 is inhibited by the peptide GsMTx4. *Biochemistry.* 50:6295–6300.
7. Bae, C., R. Gnanasambandam, …, P. A. Gottlieb. 2013. Xerocytosis is caused by mutations that alter the kinetics of the mechanosensitive channel PIEZO1. *Proc. Natl. Acad. Sci. USA.* 110:E1162–E1168.
8. Gottlieb, P. A., C. Bae, and F. Sachs. 2012. Gating the mechanical channel Piezo1: a comparison between whole-cell and patch recording. *Channels (Austin).* 6:282–289.
9. Rawicz, W., B. A. Smith, …, E. Evans. 2008. Elasticity, strength, and water permeability of bilayers that contain raft microdomain-forming lipids. *Biophys. J.* 94:4725–4736.
10. Albuisson, J., S. E. Murthy, …, A. Patapoutian. 2013. Dehydrated hereditary stomatocytosis linked to gain-of-function mutations in mechanically activated PIEZO1 ion channels. *Nat. Commun.* 4:1884.
11. Andolfo, I., S. L. Alper, …, A. Iolascon. 2013. Multiple clinical forms of dehydrated hereditary stomatocytosis arise from mutations in PIEZO1. *Blood.* 121:3925–3935, S1–S12.
12. Suchyna, T. M., S. R. Besch, and F. Sachs. 2004. Dynamic regulation of mechanosensitive channels: capacitance used to monitor patch tension in real time. *Phys. Biol.* 1:1–18.
13. Suchyna, T. M., and F. Sachs. 2007. Mechanosensitive channel properties and membrane mechanics in mouse dystrophic myotubes. *J. Physiol.* 581:369–387.
14. Ostrow, K. L., A. Mammoser, …, P. A. Gottlieb. 2003. cDNA sequence and in vitro folding of GsMTx4, a specific peptide inhibitor of mechanosensitive channels. *Toxicon.* 42:263–274.
15. Suchyna, T. M., V. S. Markin, and F. Sachs. 2009. Biophysics and structure of the patch and the gigaseal. *Biophys. J.* 97:738–747.
16. Spagnoli, C., A. Beyder, …, F. Sachs. 2008. Atomic force microscopy analysis of cell volume regulation. *Phys. Rev. E Stat. Nonlin. Soft Matter Phys.* 78:031916.
17. Chiang, C. S., A. Anishkin, and S. Sukharev. 2004. Gating of the large mechanosensitive channel in situ: estimation of the spatial scale of the transition from channel population responses. *Biophys. J.* 86:2846–2861.
18. Nomura, T., C. G. Cranfield, …, B. Martinac. 2012. Differential effects of lipids and lyso-lipids on the mechanosensitivity of the mechanosensitive channels MscL and MscS. *Proc. Natl. Acad. Sci. USA.* 109:8770–8775.
19. Sukharev, S. I., W. J. Sigurdson, …, F. Sachs. 1999. Energetic and spatial parameters for gating of the bacterial large conductance mechanosensitive channel, MscL. *J. Gen. Physiol.* 113:525–540.
20. Ursell, T., A. Agrawal, and R. Phillips. 2011. Lipid bilayer mechanics in a pipette with glass-bilayer adhesion. *Biophys. J.* 101:1913–1920.
21. Opsahl, L. R., and W. W. Webb. 1994. Lipid-glass adhesion in gigasealed patch-clamped membranes. *Biophys. J.* 66:75–79.
22. Bowman, C. L., P. A. Gottlieb, …, F. Sachs. 2007. Mechanosensitive ion channels and the peptide inhibitor GsMTx-4: history, properties, mechanisms and pharmacology. *Toxicon.* 49:249–270.
23. Horovitz, A. 1996. Double-mutant cycles: a powerful tool for analyzing protein structure and function. *Fold. Des.* 1:R121–R126.